15 Apr 2012

On the Measurement of Gas Holdup Distribution Near the Region of Impeller in a Gas-Liquid Stirred Rushton Tank by Means of Γ-CT

Li na Kong

Wei Li

Lu chang Han

Yue jin Liu

et. al. For a complete list of authors, see https://scholarsmine.mst.edu/che_bioeng_facwork/1263

Recommended Citation

L. n. Kong et al., "On the Measurement of Gas Holdup Distribution Near the Region of Impeller in a Gas-Liquid Stirred Rushton Tank by Means of Γ-CT," *Chemical Engineering Journal*, vol. 188, pp. 191 - 198, Elsevier, Apr 2012.
The definitive version is available at https://doi.org/10.1016/j.cej.2012.02.023

Chemical Engineering Journal 188 (2012) 191–198

Contents lists available at SciVerse ScienceDirect

Chemical Engineering Journal

journal homepage: www.elsevier.com/locate/cej

On the measurement of gas holdup distribution near the region of impeller in a gas–liquid stirred Rushton tank by means of γ-CT

Li-na Kong[a], Wei Li[a], Lu-chang Han[a], Yue-jin Liu[a,*], He-an Luo[a], Muthanna Al Dahhan[b], Milorad P. Dudukovic[b]

[a] School of Chemical Engineering, Xiangtan University, Xiangtan, 411105, China
[b] Chemical Reaction Engineering Laboratory, Washington University in St. Louis, MO 63130, USA

ARTICLE INFO

Article history:
Received 14 September 2011
Received in revised form 7 February 2012
Accepted 8 February 2012

Keywords:
Measurement
Gas holdup distribution
Near the region of impeller
Rushton tank
γ-CT

ABSTRACT

Three flow patterns of flooding, loading and complete recirculation in a gas–liquid stirred Rushton tank were identified based on experimental observation. The gas–liquid system was composed of air and water. Under different operating conditions of gas flow rate and impeller rotating speed, the distribution of gas holdup near the region of impeller was measured using a γ-CT scan method. Both quantitative digital distribution curves of gas holdup and their qualitative color CT images were obtained. At the region of impeller, there was a convex characteristic peak of gas holdup distribution both in radial and in axial directions, and with the region being gradually away from the impeller, the distribution of gas holdup became flatter. The values of gas holdup in S33 regime were a little higher than those in L33 regime. Higher impeller rotating speed had some effect on the increasing of gas holdup at the region of higher axial height. The experimental measurement results were basically consistent with those previously published by Bombač. The hole number and diameter of sparger had little influence on the distribution of gas holdup, while the sparger's installed height had significant influence on them. When the sparger was installed close to the bottom of Rushton tank, a comparatively smoother distribution of gas holdup above the space of impeller could be obtained. The research results in this paper were useful for better understanding of gas holdup distribution near the region of impeller of Rushton tank, and could also provide experimental data for CFD simulation.

1. Introduction

The gas–liquid hydrodynamics behavior, such as the dispersion and mixing of gas–liquid system in a gas–liquid stirred Rushton tank exhibited different flow patterns with the varying hardware (the tank scale, the impeller and sparger's details) and operating conditions (the flow rate of gas and the rotating speed of impeller) [1]. The gas–liquid flow generated by the blades of rotating impeller interacted with each other and formed some trailing vortices behind the blades of impeller, such as RC (ragged cavity structures), VC (vortex clinging cavities), L33 (three large and three small cavities) and S33 (three large and three clinging cavities) [2]. The size and shape of these cavities were used to identify different flow regimes [3]. Some research efforts had been spent on the identification of flow regimes [1–6]. For example, Nienow [4] and Warmoeskerken [6] presented a flow regime map based on the gas-filled cavity structures developed behind the blades of impeller. On which, three flow patterns of flooding, loading and complete recirculation were identified and the normally operated loading pattern was characterized in the presence of L33–S33 regimes [3]. These different flow patterns reflected different the dispersion, mixing and flow behavior of gas–liquid system in Rushton tank. Although there were some research on them [1–6], the relationship among the flow regime, flow pattern, hardware and operating condition was not yet adequately understood.

Different measurement techniques had been developed to measure the flow regimes near the region impeller of Rushton tank, which included the global measurement technique combined with visual observation [7–9], the hydrophone [10], the torque and pressure sensor [2], the resistivity probe [11–14], and so on [15–17]. However, most of them were intrusive and point measurement. Some works laid stress only on the identification and transition of flow regimes [4,6,10,12,14], and the detailed information of gas holdup distribution near the impeller of region were limited [3,10,12,14].

CT was a non-invasive and tomography measurement method, which was used in the detection of gas holdup distribution of gas–liquid system or solid void distribution of gas–solid system [18,19]. Recently, Liu [20] carried out a research on the distribution of gas holdup and CT image in a gas–liquid stirred Rushton tank

* Corresponding author. Tel.: +86 73 58293284; fax: +86 731 58293284.
E-mail address: xdlyj@163.com (Y.-j. Liu).

1385-8947/$ – see front matter © 2012 Elsevier B.V. All rights reserved.
doi:10.1016/j.cej.2012.02.023

Nomenclature

D_T	tank diameter (mm)
D_I	impeller diameter (mm)
H	tank height (mm)
Z	axial height (mm)
n	impeller rotational speed (rps)
q	gas-flow rate (L/min)
Fl	Flow number, $Fl = q/(nD_T^3)$ (dimensionless)
Fr	Froude number, $Fr = n^2 D_T/g$ (dimensionless)
g	gravity (m/s^2)

Subscripts

i	particle group i
j	particle group j

using the CT scan method. However, Liu's research only focused on the influence of gas flow rate and impeller rotating speed on the distribution of gas holdup at 3/4 static liquid height, and the information of gas holdup distribution near the region of impeller had not been reported.

The current work attempted to obtain the distribution of gas holdup near the region of impeller using the CT scan method. The influence of sparger's hole number, diameter and location on the distribution of gas holdup near the region of impeller was also examined.

2. Experiment

2.1. Experiment facilities

The Rushton tank was a cylindrical perspex tank of D_T = 200 mm diameter with four baffles of width D_T/12.5, and a six-blade Rushton impeller of diameter D_T/3 with the blade height D_T/15 and width D_T/12. A shaft of diameter $3D_T$/100 connected the impeller, which was set at the axial height of D_T/3. A ring sparger of $0.315D_T$ diameter with two types of equidistant small holes (8 holes of diameter 1.5 mm and 16 holes of diameter 0.5 mm) was used, and the sparger' off-bottom clearance was D_T/20. The gas–liquid system was composed of air and water. The whole geometry of Rushton tank was depicted in Fig. 1.

The CT set-up consisted of seven fan-arrayed NaI (Tl) detectors with a span of 5° between each other, and a 100 mCi lead shielded ^{137}Cs source located at the opposite central point of the fan-arrayed seven detectors. The seven NaI (Tl) detectors and ^{137}Cs source were installed together on a ring-shaped plate, which could both rotate and moved up and down around the Rushton tank using two stepper motors. A thick lead shielding in front of source was used to make γ-ray emit in the form of fan beam, and in front of each detector, a lead collimator was used to collect γ-ray. The CT set-up was illustrated in Fig. 2. More details about it could be found in the related references [20,21].

2.2. CT scan measurement

After fixing the CT set-up at some axial height of Rushton tank, first, the seven fan-arrayed detectors made a fan-movement of total 4.8° at a clearance of 0.2° around the source from one side to another side of the Rushton tank, so as to acquire 25 independent projections for each detector in a view scan, and then quickly rotated back to their original positions. Then, the ring-shaped plate of seven fan-arrayed detectors and ^{137}Cs source together circum-rotated 3.6° around the Rushton tank to begin a next view scan, until 100 views were acquired in this way. Finally, a total of 17,500 projections ($25 \times 7 \times 100$) were acquired in a 360° circle scanning range to meet the need of enough projections through per pixel for CT image reconstruction of gas holdup distribution.

According to the spatial resolution of CT set-up, the cross-section of Rushton tank was divided into 10,000 pixel units of 2 mm × 2 mm. Through processing of the massive random statistical attenuation signals of 17,500 projections, an E–M algorithm based on the principles of maximum likelihood [22,23] was used to obtain a time-averaged value of gas holdup in each pixel. Thus, 10,000 time-averaged values of gas holdup were obtained on the cross-section of Rushton tank, on which the CT color image could be formed. Then, a radial distribution curve of gas holdup with dimensionless radius could be obtained by averaging time-averaged values of gas holdup in each pixel along different concentric annuli at an interval of 0.02 dimensionless radius.

Changing the CT set-up at different axial heights of Rushton tank, both the color CT images of gas holdup distribution and their radial distribution curves of gas holdup with dimensionless radius were obtained through CT scan. Finally, an axial distribution curve of

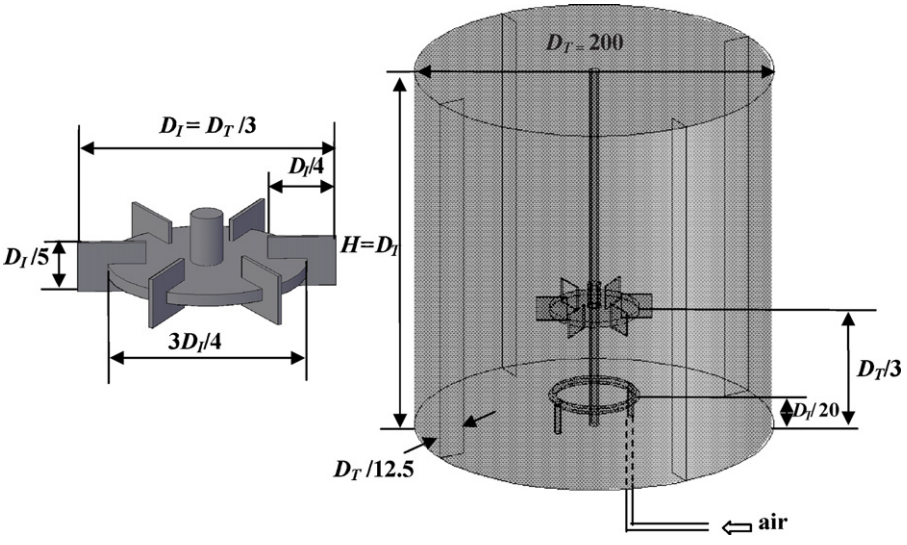

Fig. 1. The Rushton tank.

Table 1
The experimental conditions for flow pattern.

	Gas flow rate (L/min)		
	9.44	18.88	28.32
Flooding to loading	350* (*Fl* = 0.09, *Fr* = 0.23)	470* (*Fl* = 0.14, *Fr* = 0.42)	530* (*Fl* = 0.18, *Fr* = 0.53)
Loading	500* (*Fl* = 0.06, *Fr* = 0.47)	600* (*Fl* = 0.11, *Fr* = 0.68)	640* (*Fl* = 0.15, *Fr* = 0.77)
Complete recirculation	800* (*Fl* = 0.04, *Fr* = 1.21)	800* (*Fl* = 0.08, *Fr* = 1.21)	800* (*Fl* = 0.12, *Fr* = 1.21)

* The rotating speed of impeller (rpm).

gas holdup could be obtained by averaging values of gas holdup at different axial heights of Rushton tank.

3. Result and discussion

3.1. The flow regime and flow pattern

Based on the cavity structures developed behind the blades of impeller, the flow regime map in Fig. 3 was given in dimensionless flow number *Fl* (the ratio of the sparger rate of gas to the rate of pumped liquid), and dimensionless Froude number *Fr* (the ratio of inertial or centrifugal force of moving-tangentially outward liquid near the edge of rotating impeller to the gravitational force).

When the rotating speed of impeller increased from zero at a given gas flow rate, first, the flooding was formed (Fig. 4a), where the gas sparging produced and dominated the bubble column of rising gas around the shaft. When the rotating speed of impeller further increased to some critical speed, the flooding was suddenly changed into the loading, where gas bubbles were well distributed above the space of impeller (Fig. 4b). When the rotating speed of impeller further increased over the critical speed, the complete recirculation loops of gas bubbles were formed both above and below the impeller (Fig. 4c), which was caused by the splitting of discharged flow from the impeller, upon reaching the tank wall in radial direction. At this time, the impeller dominated the dispersion effects of rising gas from the sparging. These flow patterns are marked on the flow regime map in Fig. 3, and the corresponding experimental condition is listed in Table 1.

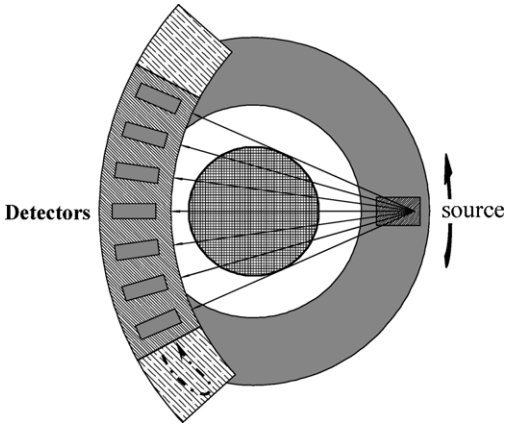

Fig. 2. The scan sketch of γ-CT.

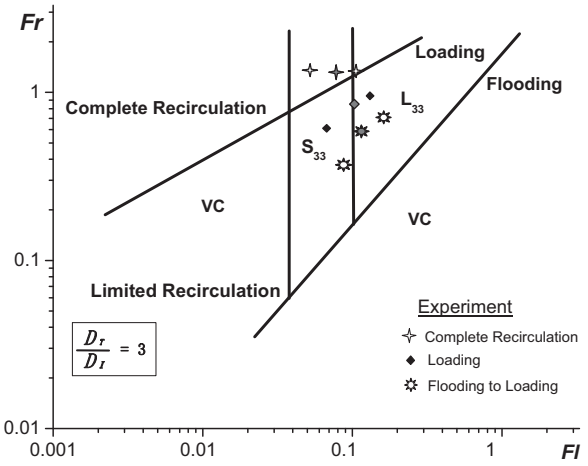

Fig. 3. The flow regime map.

Table 2
The experimental condition of axial gas holdup distribution.

Regime	The current work	Bombač's work
L33	*n* = 470 rpm, *q* = 18.88 L/min	*n* = 265.8 rpm, *q* = 100.2 L/min
L33–S33	*n* = 600 rpm, *q* = 18.88 L/min	–
S33	*n* = 800 rpm, *q* = 18.88 L/min	*n* = 376.2 rpm, *q* = 100.2 L/min

Comparing the experiment results with the flow regime map, it could be seen that the experiment results basically corresponded to the flow regime map. The normally operated loading pattern was characterized by the presence of L33–S33 regimes [3]. This was because that in the pattern of loading, massive gas cavities could produce and develop behind the blades of impeller, and a variety of gas bubbles mainly occurred near the region of impeller. To obtain comprehensive information of gas holdup distribution near the region of impeller, three typical experimental points in Fig. 3 were chosen for CT scan in detail.

3.2. Axial gas holdup distribution

Under the experimental condition listed in Table 2, the axial distributions of gas holdup in Rushton tank were obtained according to the method mentioned in Section 2.2. The results were plotted in Fig. 5. Compared with Bombač's experimental results [3], it could be seen that, on the whole, there were similar axial distributions of gas holdup in L33–S33 regimes, although both experimental conditions of gas flow rate and impeller rotating speed were quite different. Gas bubbles significantly appeared near the region of impeller and exhibited a convex characteristic peak at this region. Below the impeller, only little gas bubbles appeared. With the increase in axial height, gas holdup distribution became flatter. Gas holdup in S33 regime was a little higher than that in L33 regime. Although the gas flow rate here was lower than that in Bombač's experiment, higher gas holdup was still obtained. It was perhaps because higher impeller rotating speed was adopted.

3.3. Radial gas holdup distribution

3.3.1. Digital distribution curve

After fixing the gas flow rate of 18.88 L/min, under different axial heights (*Z*/*H* = 1/3, 4/9 and 1/2) and different impeller rotating speeds (470, 600, 800 rpm), the radial distributions of gas holdup near the region of impeller were obtained using CT scan measurement. The radial digital distribution curves of gas holdup are shown in Fig. 6.

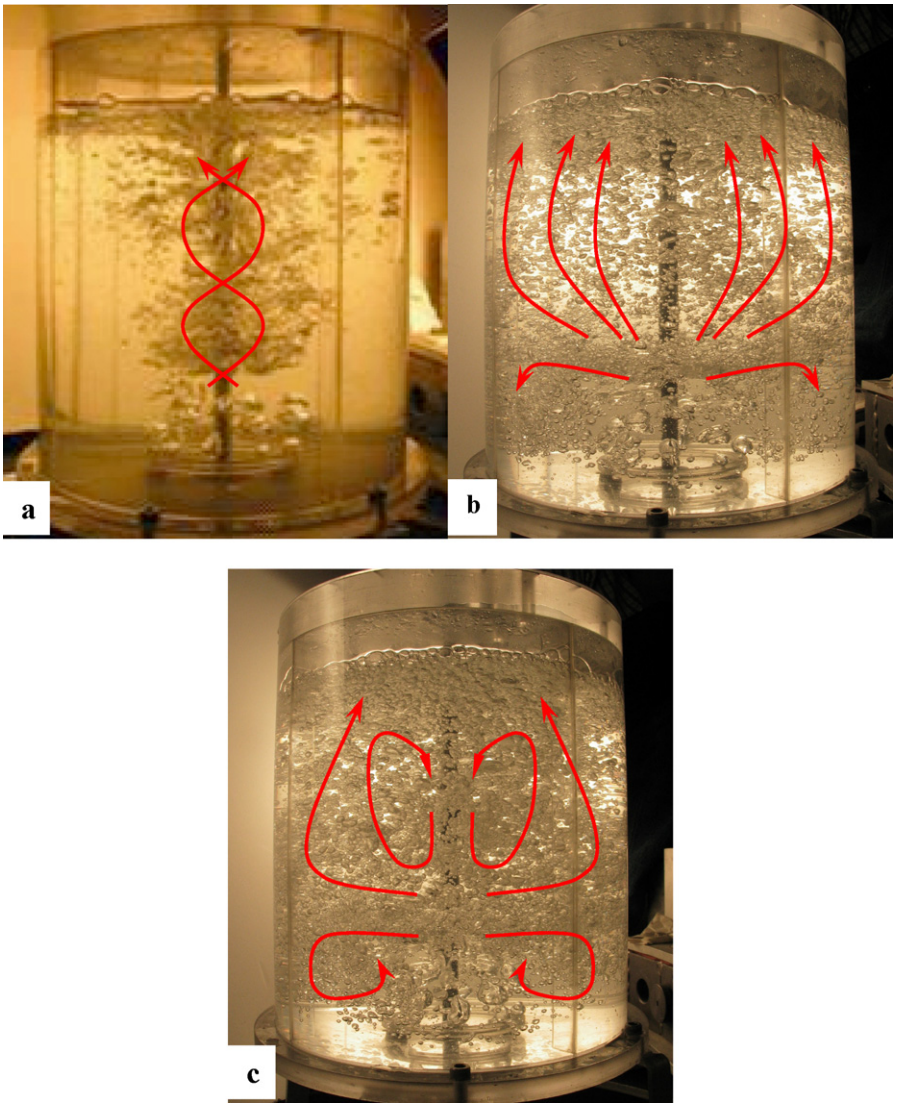

Fig. 4. The flow patterns at flow rate q = 18.88 L/min: a – flooding, b – loading, and c – complete recirculation.

At the same axial height, the radial distribution curves of gas holdup were similar. At the central region of impeller, because of the block-down effect of impeller disk on the rising of gas bubbles emitting from the ring sparger, gas holdup was quite low.

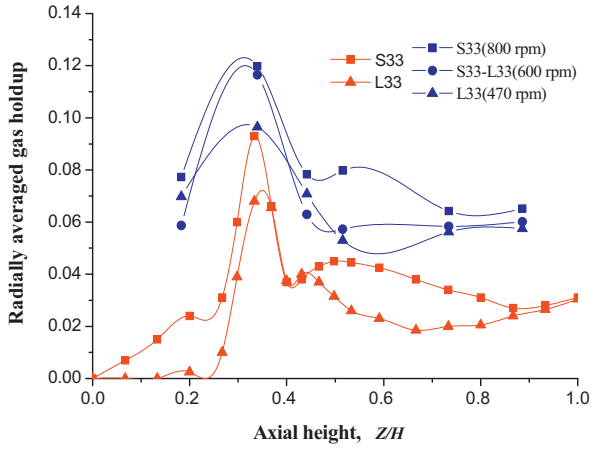

Fig. 5. The axial gas holdup distribution.

When the dimensionless radius was over 0.2, gas holdup began to increase significantly and exhibited different gas holdup distributions at different axial heights. With the increase in axial height, this convex characteristic peak of gas holdup distribution became diverging and moved away from the edge of impeller blades.

At the axial impeller height (Z/H = 1/3), the convex characteristic peak of gas holdup distribution appeared at the edge of impeller blades (0.34 dimensionless radius). After experiencing the peak, gas holdup decreased sharply and became flatter with the increase in dimensionless radius. Under three different impeller rotating speeds (470, 600, 800 rpm), the distributions of gas holdup were nearly over-lapped, and only after the dimensionless radius reached 0.47, gas holdup was a little different. Higher gas holdup appeared in S33 regime, lower in L33 regime, and the middle in S33–L33 regimes. At the axial height of Z/H = 4/9, only when the dimensionless radius was in the range of 0.25–0.5, gas holdup in S33 regime was obviously higher than those in other two regimes. At the axial height of Z/H = 1/2, gas holdup in S33 regime was obviously higher than those in other two regimes. The above phenomena showed that higher impeller rotating speed had some effect on the increasing of gas holdup at the region of higher axial height.

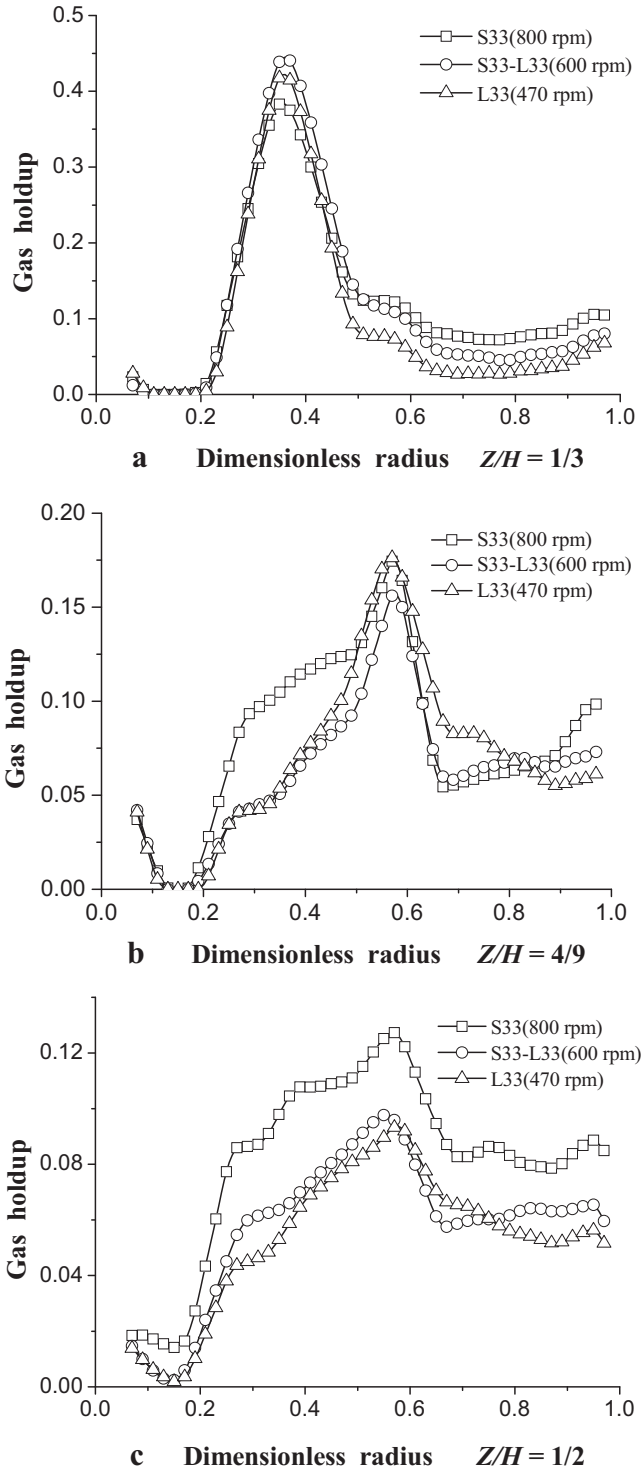

Fig. 6. The radial gas holdup distributions at different axial heights (Z/H): a – 1/3, b – 4/9, and c – 1/2 with 18.88 L/min of gas flow rate.

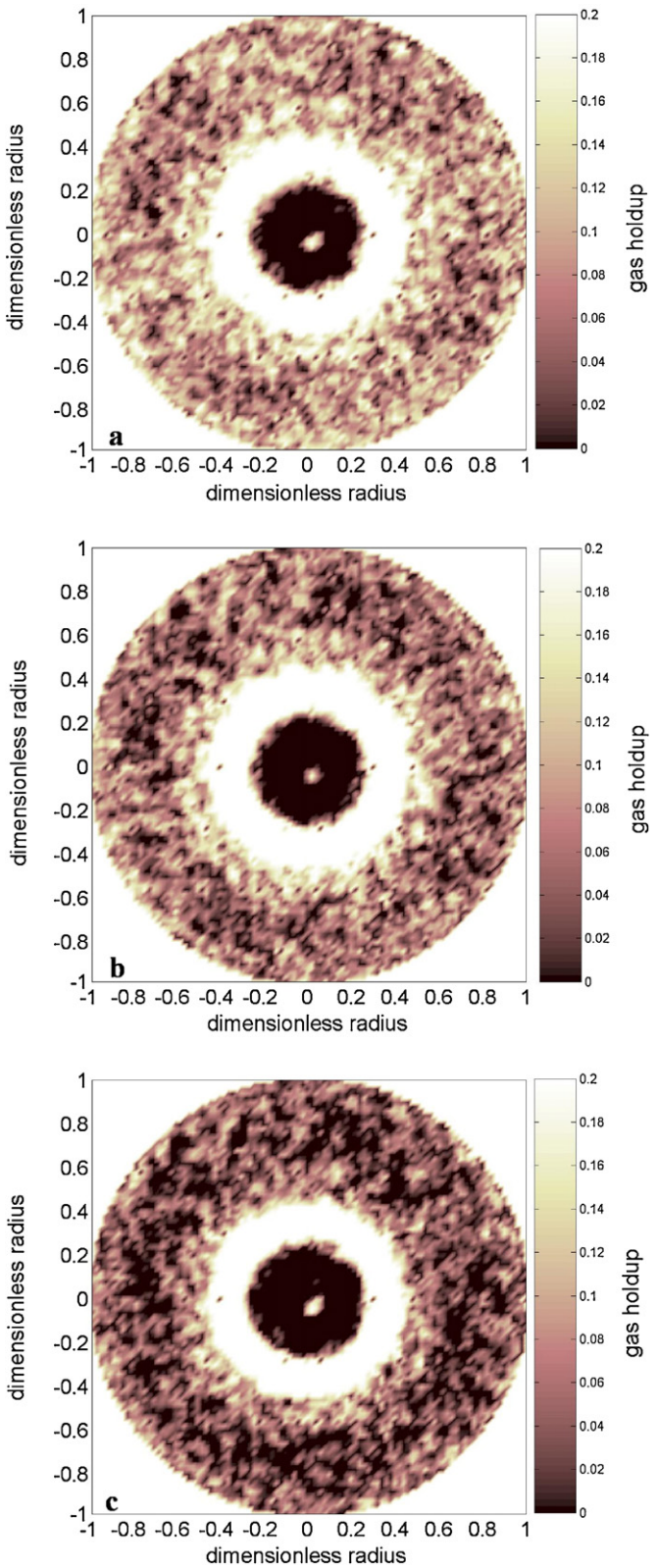

Fig. 7. The CT images of gas holdup distribution at $Z/H = 1/3$: a – S33, b – S33–L33, and c – L33. (For interpretation of the reference to color in the text, the reader is referred to the web version of the article.)

3.3.2. CT images

The corresponding color CT images of gas holdup distributions in Fig. 6 are shown in Figs. 7–9. These CT images could clearly demonstrate the cross-sectional distributions of gas holdup and their changes. The darker the color of CT image was, the smaller the value of gas holdup was. A black circle plane appeared at the central region of CT images, which meant that gas holdup at this region was quite low and proved the block-down effect of impeller disk on the gas bubbles rising from the sparger. At the region of

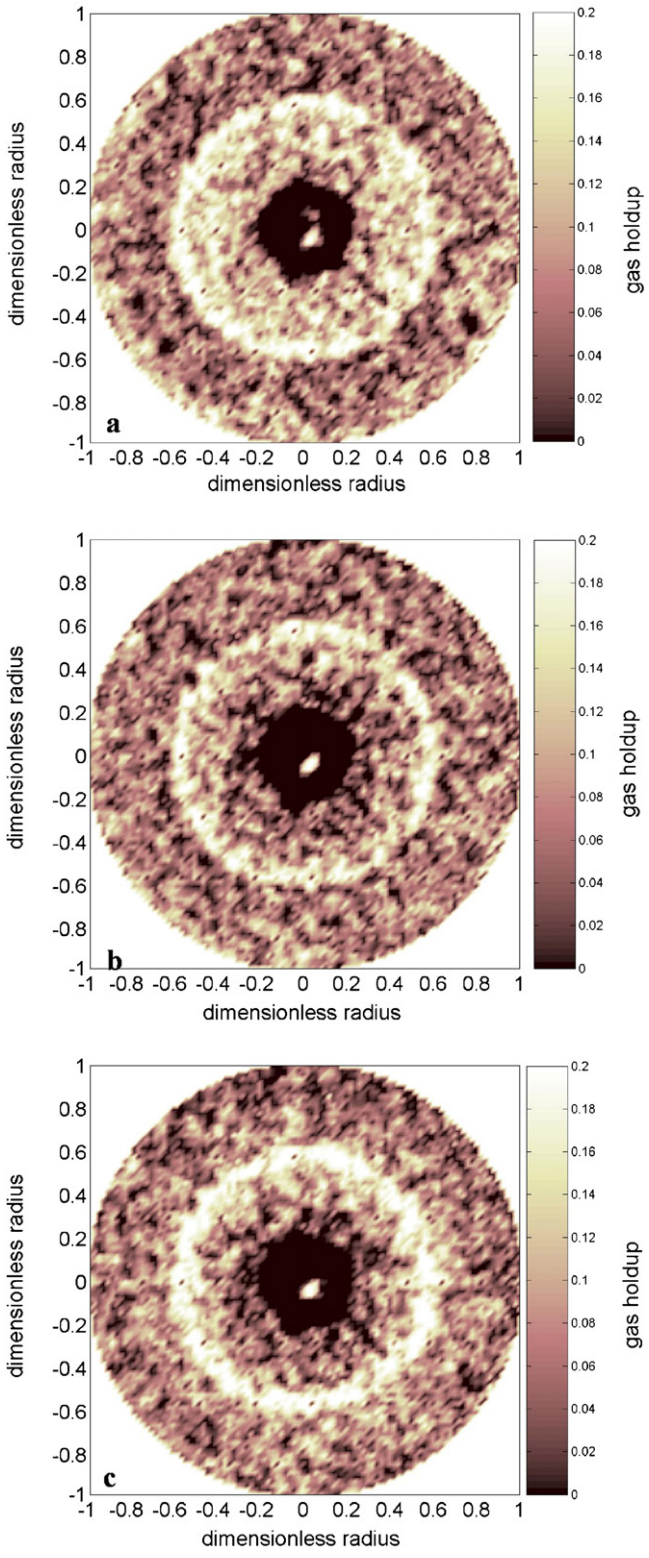

Fig. 8. The CT images of gas holdup distribution at $Z/H = 4/9$: a – S33, b – S33–L33, and c – L33. (For interpretation of the reference to color in the text, the reader is referred to the web version of the article.)

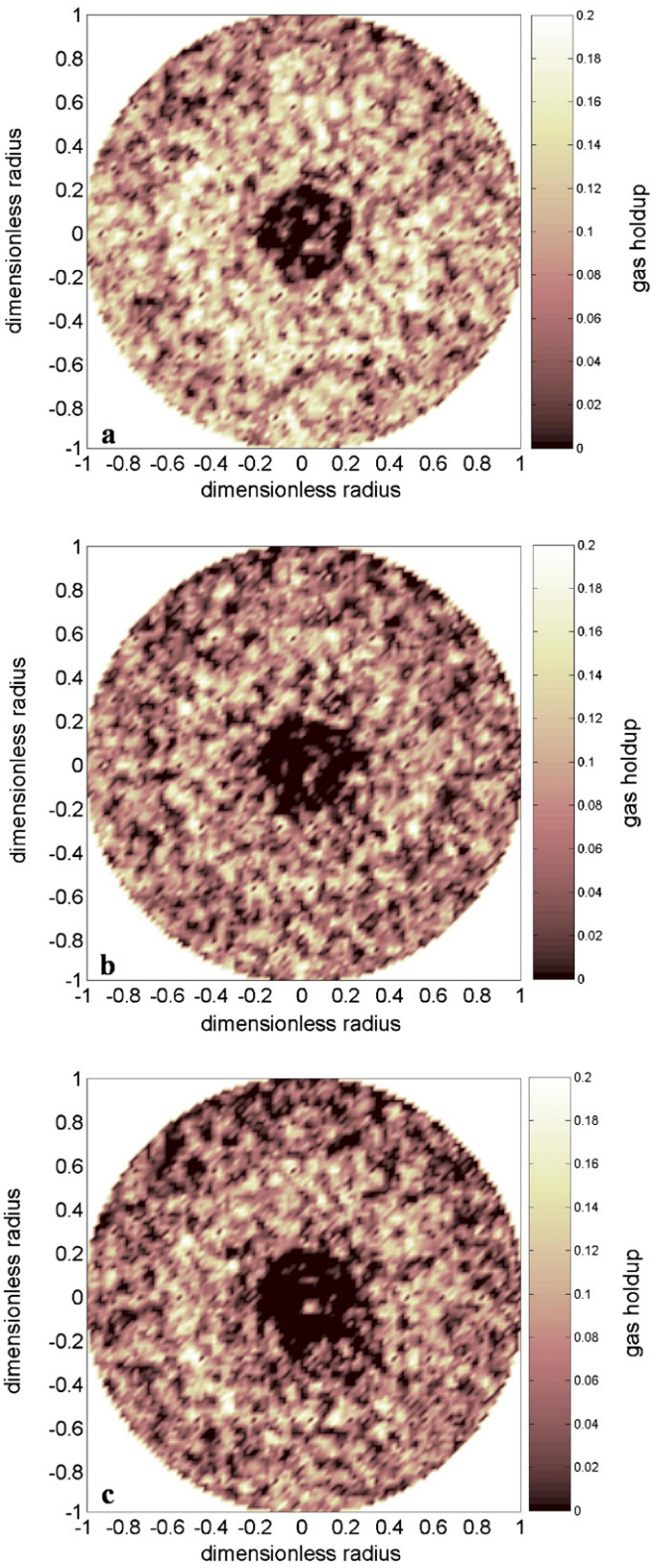

Fig. 9. The CT images of gas holdup distribution at $Z/H = 1/2$: a – S33, b – S33–L33, and c – L33. (For interpretation of the reference to color in the text, the reader is referred to the web version of the article.)

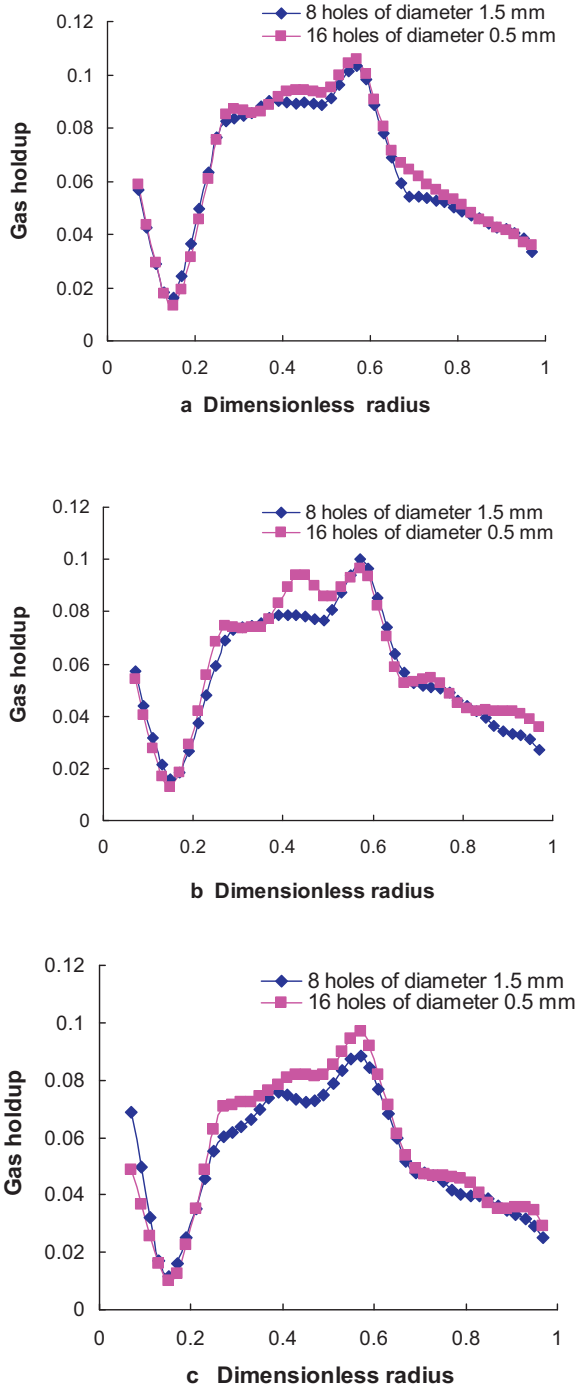

Fig. 10. The influence of sparger's hole number and diameter on radial gas holdup distribution in L33–S33 regimes at $Z/H = 2/3$: a – S33, b – S33–L33, and c – L33.

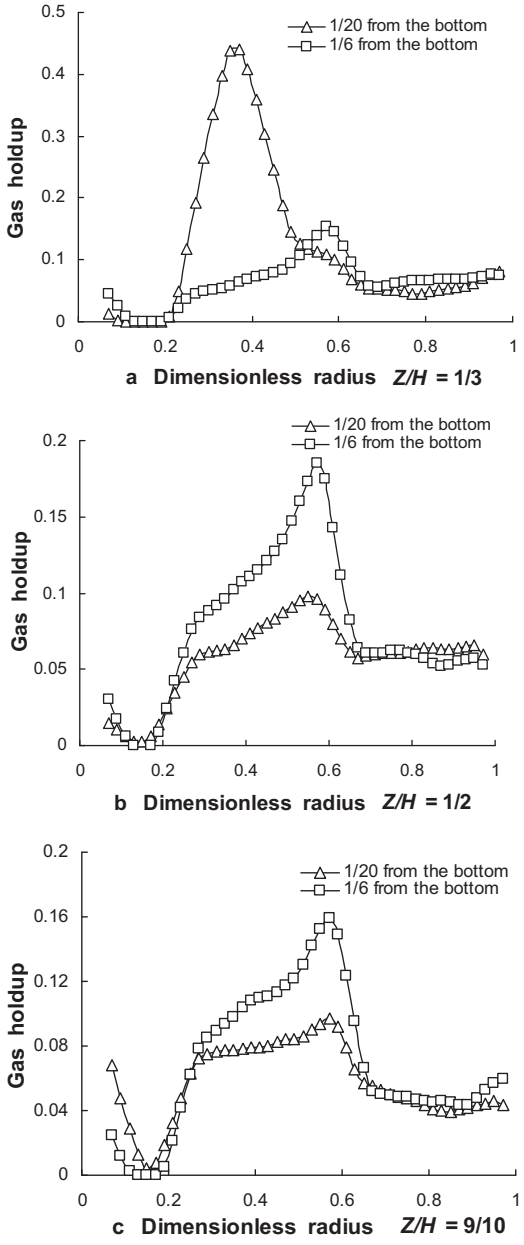

Fig. 11. The influence of sparger location on gas holdup distribution in S33–L33 regimes at different axial heights (Z/H): a – 1/6, b – 1/3, and c – 9/10.

impeller blades, a white ring area appeared, which meant that more gas bubbles existed at this region and proved the break-down effect of impeller blades on the gas bubbles rising from the sparger. With the increase in axial height, the effects of both impeller disk and impeller blades on the gas bubbles rising from the ring sparger became weak. The gray CT pixels mixed with the "black" and the "white" colors showed a comparatively uniform gas holdup distribution at the outer region of CT images. At the same axial height, the color of CT image in L33 regime was darker than that in S33 regime, which meant that more gas bubbles existed in S33 regime. The above qualitative color CT images of gas holdup distribution showed good agreements with the quantitative digital distribution curves of gas holdup.

3.4. The influence of sparger

3.4.1. The influence of sparger's hole number and diameter

With two kinds of spargers (8 holes of diameter 1.5 mm and 16 holes of diameter 0.5 mm), the radial distributions of gas holdup at four axial heights ($Z/H = 1/6$, 1/3, 2/3 and 4/9) were examined respectively, which showed that the radial distributions of gas holdup with two kinds of spargers were similar, and their changing trends were also almost the same. The typical result is shown in Fig. 10. So, the hole number and diameter of sparger had little influence on the radial gas holdup distribution.

3.4.2. The influence of sparger's installed height

When the sparger was installed at $Z/H = 1/20$ and 1/6 respectively, the radial distributions of gas holdup at three axial heights of $Z/H = 1/3$, 1/2 and 9/10 are examined in Fig. 11, which showed that the sparger's installed height had significant influence on the radial distribution of gas holdup. At the axial height of $Z/H = 1/3$, gas holdup and its distribution with the sparger's installed height at $Z/H = 1/6$ were respectively lower and smoother than those with the sparger's installed height at $Z/H = 1/20$, while at the axial heights of $Z/H = 1/2$ and 9/10, the situation was in reverse. So, in order to obtain comparatively smoother distribution of gas holdup near the region of impeller, the sparger was installed at the axial height of $Z/H = 1/20$.

4. Conclusion

Three flow patterns of flooding, loading and complete recirculation in a gas–liquid stirred Rushton tank were identified based on experimental observation. Gas bubbles mainly appeared above the space of impeller and varied greatly near the impeller region.

The distributions of gas holdup near the region impeller in Rushton tank were measured using γ-CT scan method under different operating conditions of gas flow rate and impeller rotating speed. Both quantitative digital distribution curves of gas holdup and their qualitative color CT images were obtained, which demonstrated that there was a convex characteristic peak of gas holdup distribution at the region of impeller both in radial and in axial directions. With the region being gradually away from impeller, the distribution of gas holdup became flatter. The values of gas holdup in S33 regime were a little higher than those in L33 regime. Higher impeller rotating speed had some effect on the increasing of gas holdup at the region of higher axial height. The experimental measurement results were basically consistent with those previously published by Bombač.

The hole number and diameter of sparger had little influence on gas holdup distribution, while the sparger's installed height had significant influence on them. When the sparger was installed at the axial height of $Z/H = 1/20$, a comparatively smoother distribution of gas holdup above the space of impeller could be obtained.

The research results in this paper were useful for better understanding of gas holdup distribution near the region of impeller of Rushton tank, and could also provide experimental data for CFD simulation.

Acknowledgments

The authors thank for the financial support from China Scholarship Council, CREL of Washington University in St. Louis (USA), and Specialized Research Fund for the Doctoral Program of Higher Education of China (20050530001). This work was partly supported by Hunan Provincial Natural Science Foundation (05JJ30026, 11B123) and National Natural Science Foundation of China (20776121, 21106122).

References

[1] M.M.C.G. Warmoeskerken, J.M. Smith, Description of the power curves of turbine stirred gas–liquid dispersions, in: Proceedings of the 4th European Conference on Mixing, Noordwijkerhout, BHRA Fluid Engineering, Cranfield, 1982, pp. 237–246.
[2] A. Bombač, I. Žun, B. Filipič, M. Žumer, Gas-filled cavity structures and local void fraction distribution in aerated stirred vessel, AIChE J. 43 (11) (1997) 2921–2931.
[3] A.R. Khopkar, S.S. Panaskar, Characterization of gas–liquid flows in stirred tanks using pressure and torque fluctuations, Ind. Eng. Chem. Res. 44 (2005) 3298–3311.
[4] A.W. Nienow, M.M.C.G. Warmoeskerken, J.M. Smith, M. Konno, On the flooding/loading transition and the complete dispersal condition in aerated vessels agitated by a Rushton-turbine, in: Proceedings of the 5th European Conference on Mixing, BHRA, The Fluid Engineering Centre Cranfield, Bedford, UK, 1985, pp. 143–154.
[5] V. Hudcova, V. Machon, A.W. Nienow, Gas–liquid dispersion with dual Rushton turbine impellers, Biotechnol. Bioeng. 34 (1989) 617–628.
[6] J.M. Smith, M.M.C.G. Warmoeskerken, E. Zeef, Flow conditions in vessel dispersing gases in liquids with multiple impellers, in: C.S. Ho, J.Y. Oldshue (Eds.), Biotechnology Processes, AIChE, 1987, pp. 107–115.
[7] K. Takahashi, W. McManamey, A. Nienow, Bubble size distribution in impeller region in gas sparged tank agitated by a Rushton turbine, J. Chem. Eng. Jpn. 25 (4) (1992) 427–432.
[8] V. Linek, T. Moucha, J. Sinkule, Gas–liquid mass transfer in tank stirred with multiple impellers. I. Gas liquid mass transfer characteristics in individual stages, Chem. Eng. Sci. 51 (12) (1996) 3203–3212.
[9] Z. Gao, J. Smith, H. Muller-Steinhagen, Void fraction distribution in sparged and boiling reactors with modern impeller configuration, Chem. Eng. Process. 40 (2001) 489–497.
[10] T.A. Sutter, G.L. Morrison, G.B. Tatterson, Sound spectra in an aerated agitated tank, AIChE J. 33 (4) (1987) 668–671.
[11] Y. Nagase, H. Yasui, Fluid motion and mixing in a gas–liquid contactor with turbine agitators, Chem. Eng. J. 27 (1) (1983) 37–47.
[12] A. Bombač, I. Žun, Gas-filled cavity structures and local void fraction distribution in vessel with dual impellers, Chem. Eng. Sci. 55 (2000) 2995–3001.
[13] M. Bouaifi, G. Hebrard, D. Bastoul, M. Roustan, A comparative study of gas hold-up, bubble size, interfacial area and mass transfer coefficients in stirred gas–liquid reactors and bubble columns, Chem. Eng. Process. 40 (2001) 97–111.
[14] A. Bombač, I. Žun, Individual impeller flooding in aerated tank stirred by multiple Rushton impellers, Chem. Eng. J. 116 (2) (2006) 85–95.
[15] A. Paglianti, S. Pintus, M. Giona, Time-series analysis approach for the identification of flooding/loading transition in gas–liquid stirred tank reactors, Chem. Eng. Sci. 55 (23) (2000) 5793–5802.
[16] M. Kamiwano, M. Kaminoyama, K. Nishi, D. Shirota, The measurement of bubble diameter distribution and liquid side mass transfer coefficients in a gas–liquid agitated tank using a real time, high speed image processing system, Chem. Eng. Commun. 190 (2003) 1096–1114.
[17] M. Wang, A. Dorward, D. Vlaev, R. Mann, Measurements of gas–liquid mixing in a stirred tank using electrical resistance tomography (ERT), Chem. Eng. J. 77 (2000) 93–98.
[18] D. Toye, M. Crine, P. Marchot, Imaging of liquid distribution in reactive distillation packings with a new high energy X-ray tomography, Meas. Sci. Technol. 16 (2005) 2213–2220.
[19] J. Ford, T. Heindel, T. Jensen, J. Drake, X-ray computed tomography of a gas-sparged stirred-tank reactor, Chem. Eng. Sci. 63 (2008) 2075–2085.
[20] Y.J. Liu, W. Li, L.C. Han, γ-CT measurement and CFD simulation of cross section gas holdup distribution in a gas–liquid stirred standard Rushton tank, Chem. Eng. Sci. 66 (2011) 3721–3731.
[21] S.B. Kumar, D. Moslemian, M.P. Dudukovic, A g-ray tomographic scanner for imaging of voidage distribution in two-phase flow systems, Flow Meas. Instrum. 6 (1) (1995) 61–73.
[22] C. Kak, M. Slaney, Principles of Computerised Tomographic Imaging, IEEE Press, New York, 1988.
[23] R. Maad, G.A. Johansen, Automatic weight matrix generation for gamma-ray tomography, in: Proceedings of the 3rd World Congress on Industrial Process Tomography, Banff, Canada, 2003, pp. 86–89.